Electronic Supplementary Information (ESI)

A mesoporous ionic solid with 272 $Au^{I}_{6}Ag^{I}_{3}Cu^{II}_{3}$ complex cations in a super huge crystal lattice

Hiroto Takeda, Tatsuhiro Kojima, Nobuto Yoshinari and Takumi Konno*

Department of Chemistry, Graduate School of Science, Osaka University, Toyonaka, Osaka 560-0043, Japan
konno@chem.sci.osaka-u.ac.jp

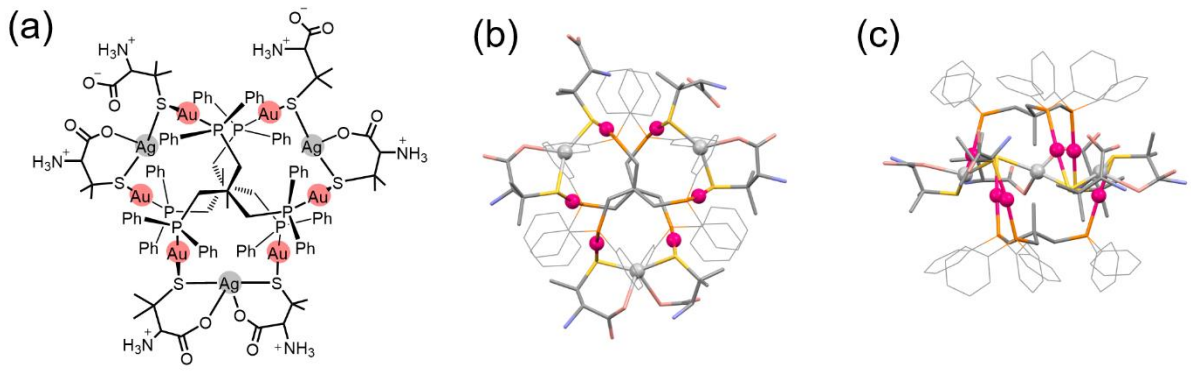

Fig. S1 Structure of $[Ag_3(D\text{-}H_3L^{Au3})_2]^{3+}$. ChemDraw structure (a). Top (b) and side (c) views of the X-ray structure of $[Ag_3(D\text{-}H_3L^{Au3})_2]^{3+}$ in $[Ag_3(D\text{-}H_3L^{Au3})_2](NO_3)_3$. One of the two crystallographically independent complex cations is presented. [Colour codes: red, Au; silver, Ag; orange, P; yellow, S; pink, O; pale blue, N; grey, C.]

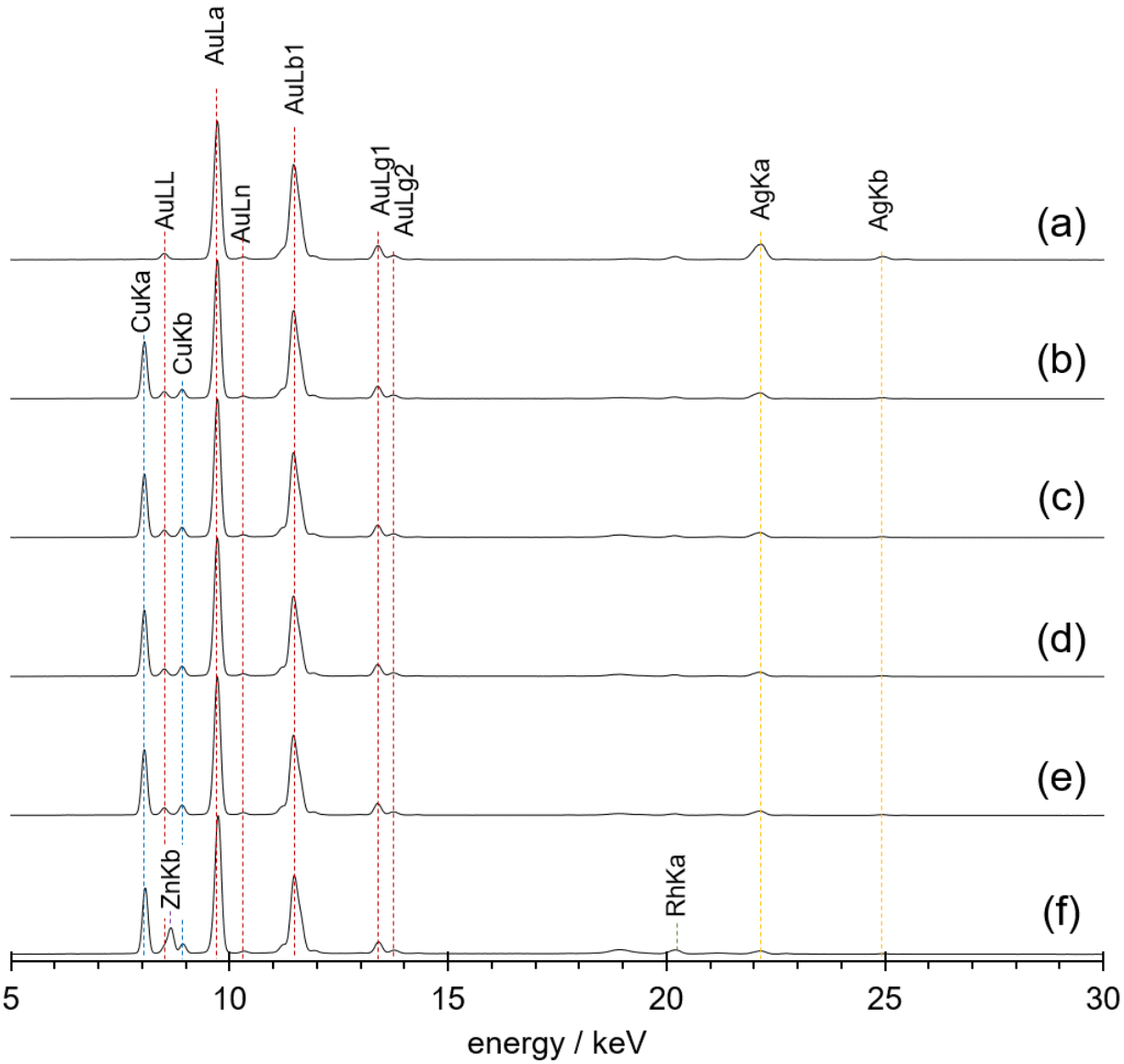

Fig. S2 X-ray fluorescence spectra. $[Ag_3(D\text{-}H_3L^{Au3})_2](NO_3)_3$ (a), **I'** (b), **I** (c), **II'** (d), **II** (e) and $\mathbf{I_{RhZn}}$ (f).

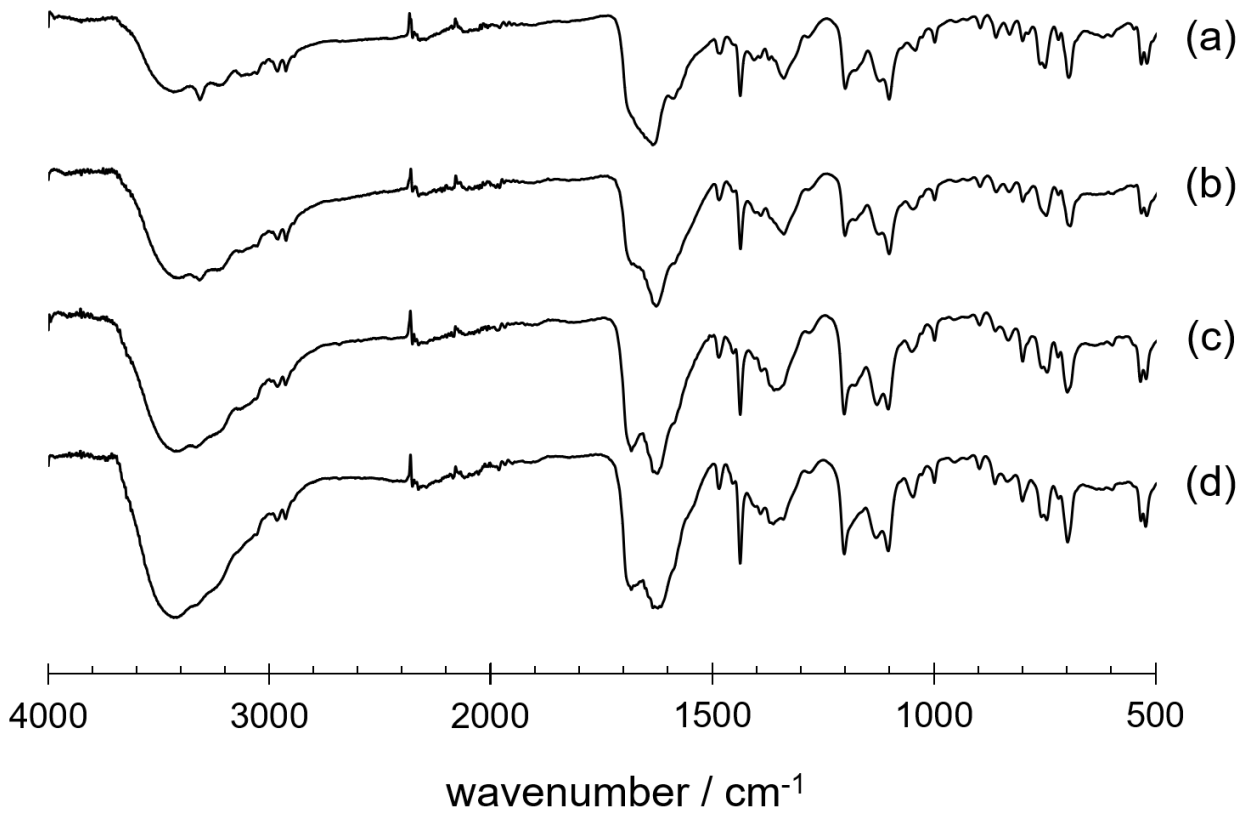

Fig. S3 IR spectra (ATR). **I'** (a), **I** (b), **II'** (c) and **II** (d).

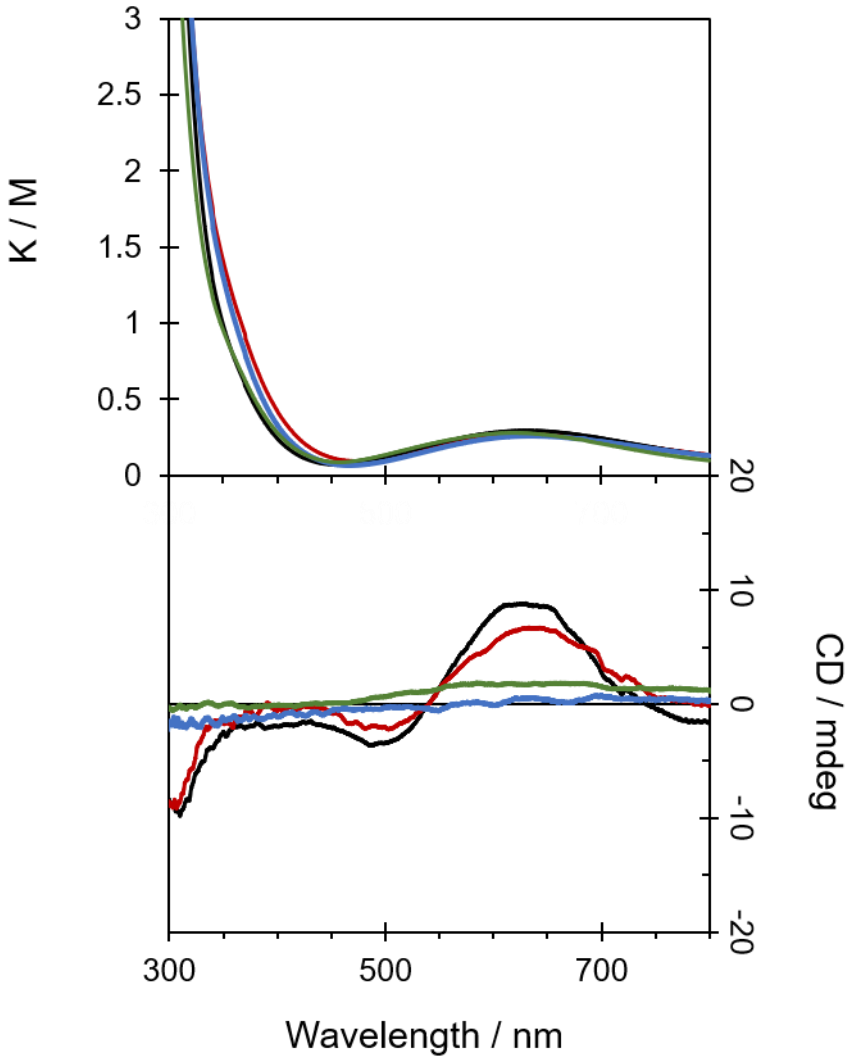

Fig. S4 Solid-state diffuse reflectance (Top) and CD spectra (bottom). **I'** (black), **I** (red) **II'** (blue) and **II** (green).

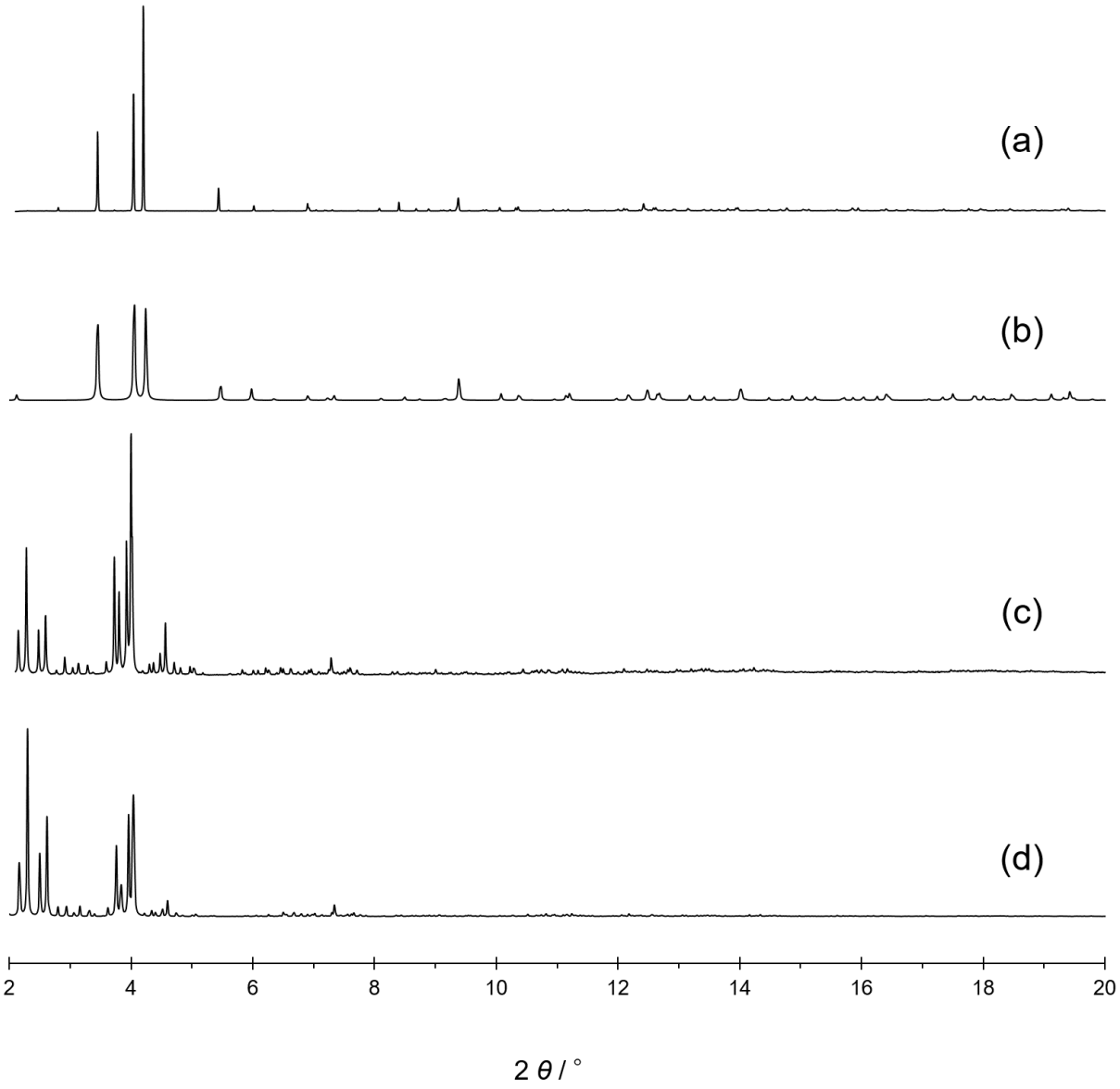

Fig. S5 Powder X-ray diffraction patterns. The observed patterns measured at room temperature (λ = 1.000 Å) for **I'** (a) and **I** (c). The simulated patterns for **I'** (b) and **I** (d).

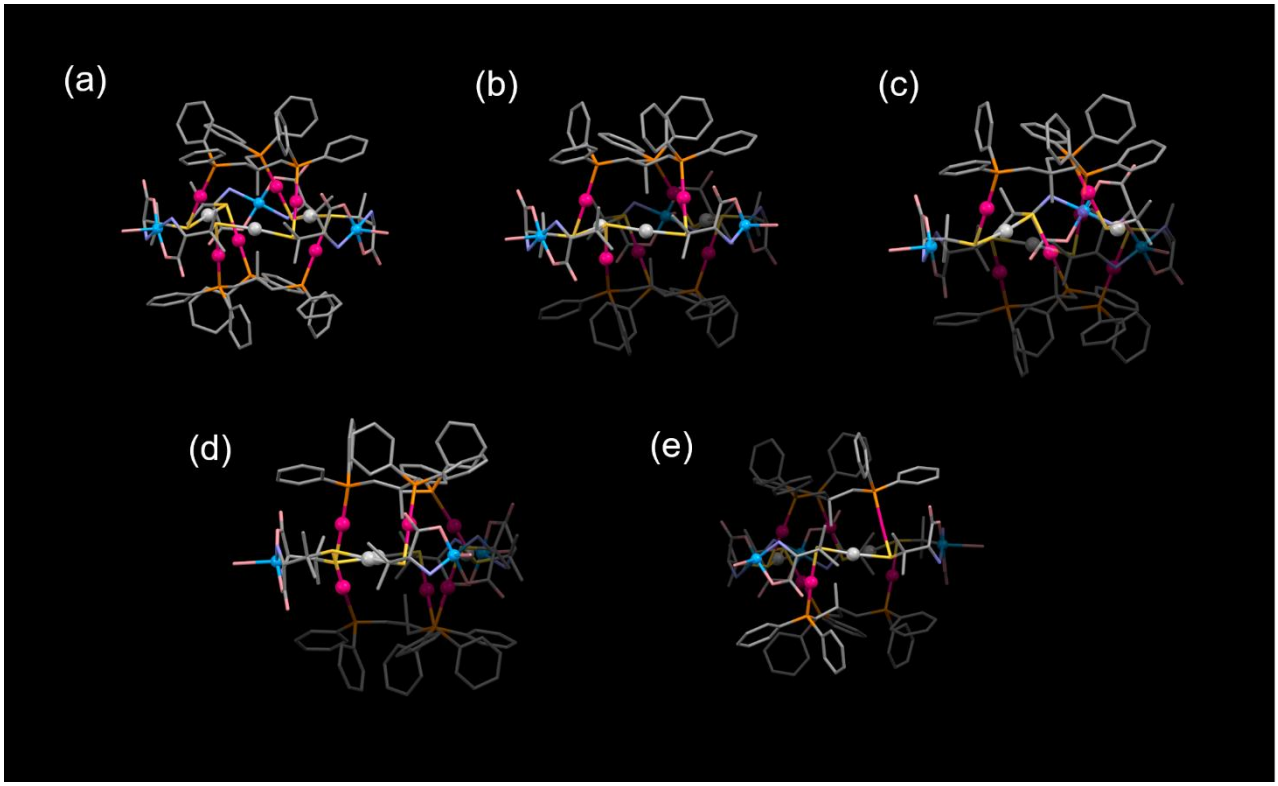

Fig. S6 Structures of the crystallographically independent $[\mathbf{1^D}]^{3+}$ complex cations in **I**. An entire $[\mathbf{1^D}]^{3+}$ complex cation (a), half cations (b, c, d) and one-third of a $[\mathbf{1^D}]^{3+}$ complex cation unit (e). Entire molecular structures are represented transparently in b-e. [Colour codes: red, Au; silver, Ag; blue, Cu; orange, P; yellow, S; pink, O; pale blue, N; grey, C.]

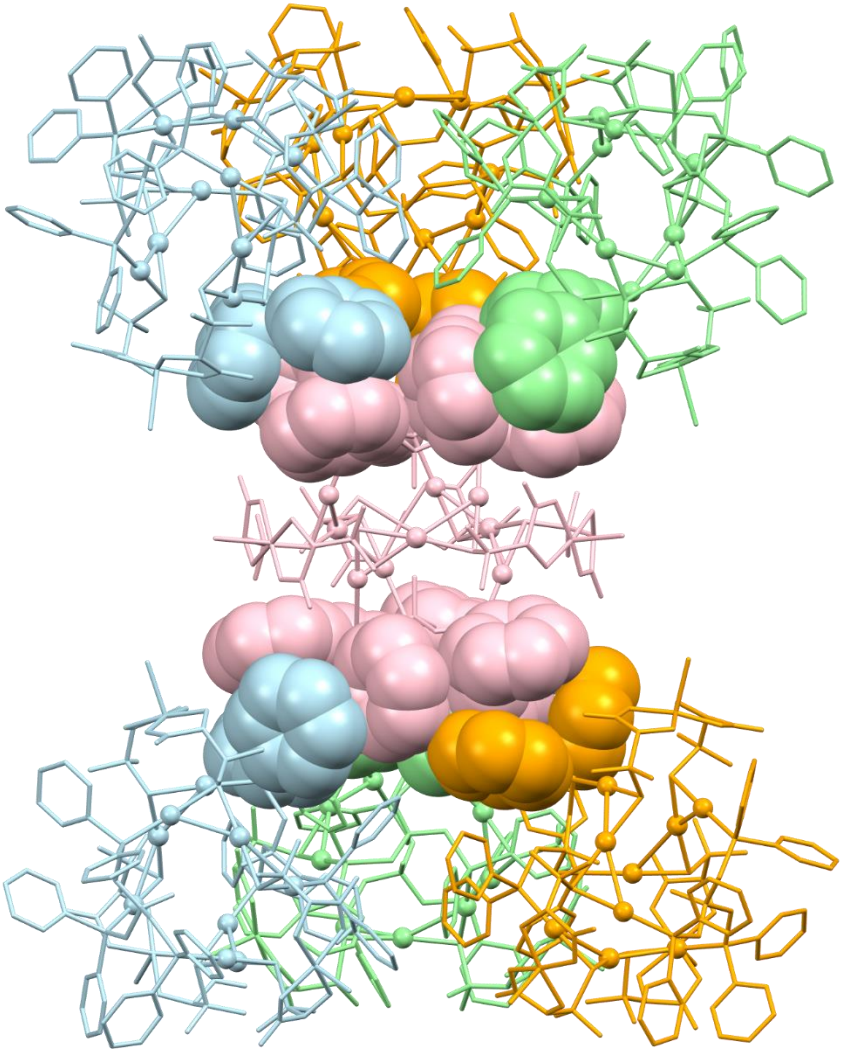

Fig. S7 Perspective view of CH···π interactions between $[\mathbf{1}^{\mathbf{D}}]^{3+}$ cations through the tdme phenyl groups in **I**.

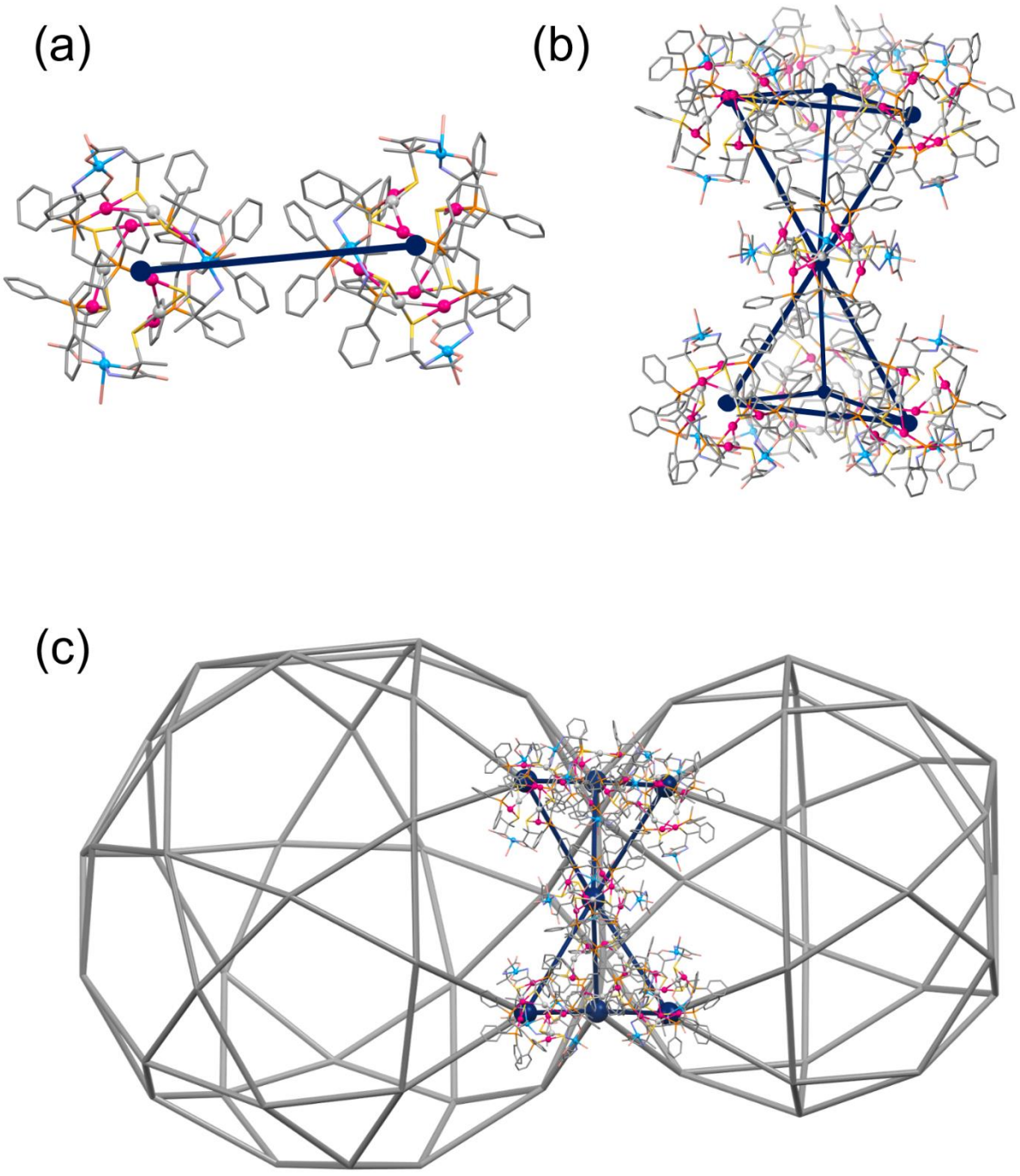

Fig. S8 Framework structure in **I**. $Au^{I}_{6}Ag^{I}_{3}Cu^{II}_{3}$ complex cations connected by CH···π contacts are represented. Connection between two complex cations (a). Vertex-sharing two tetrahedra (b). Connection between cage A with a $[3^{28}.5^{12}.6^{4}]$ face arrangement and cage B with $[3^{20}.5^{12}]$ face arrangement (c).

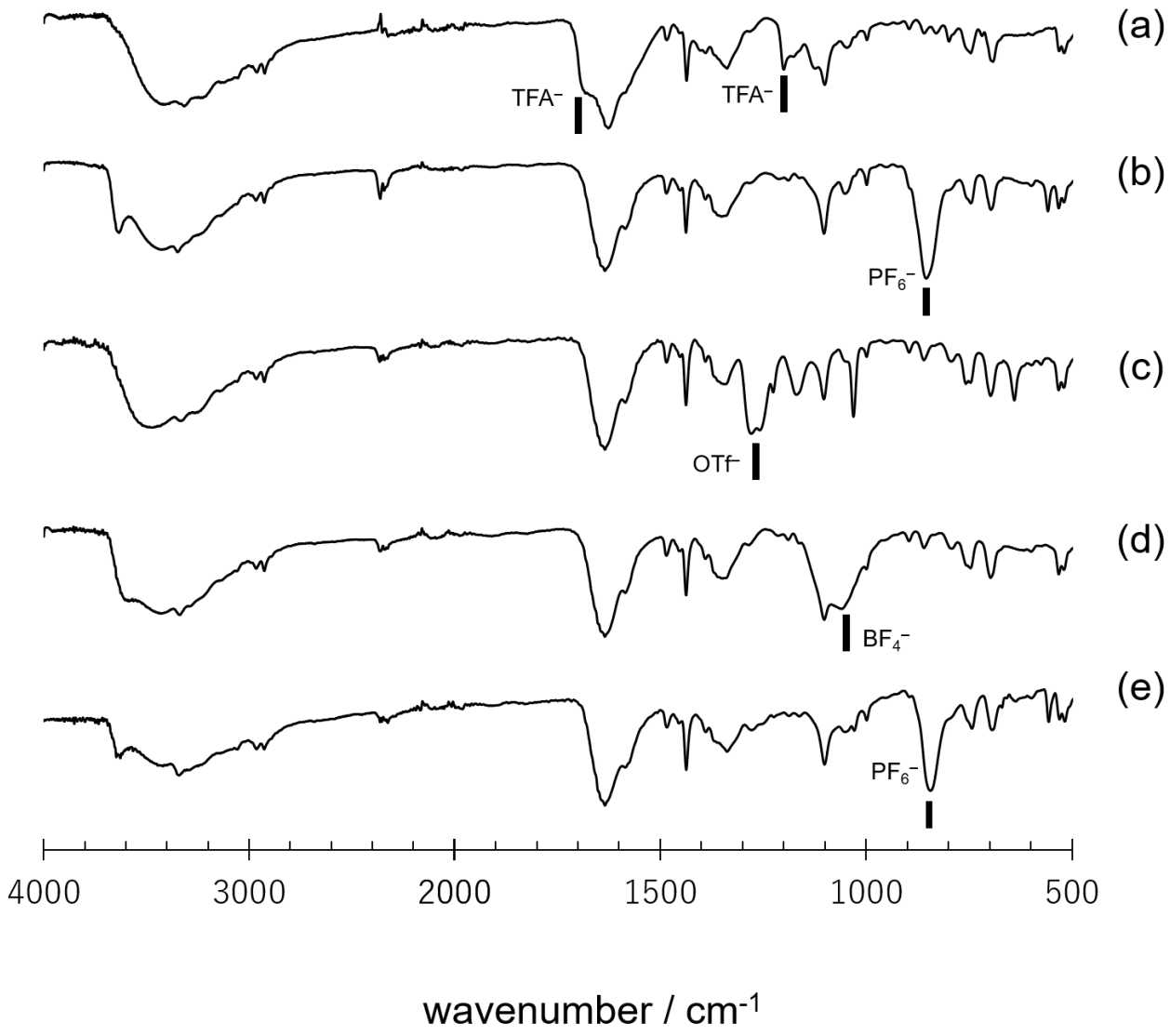

Fig. S9 IR spectra (ATR). **I** (a), $\mathbf{I_{PF6}}$ (b), $\mathbf{I_{OTf}}$ (c), $\mathbf{I_{BF4}}$ (d) and $\mathbf{I_{PF6/BF4/OTf}}$ (e).

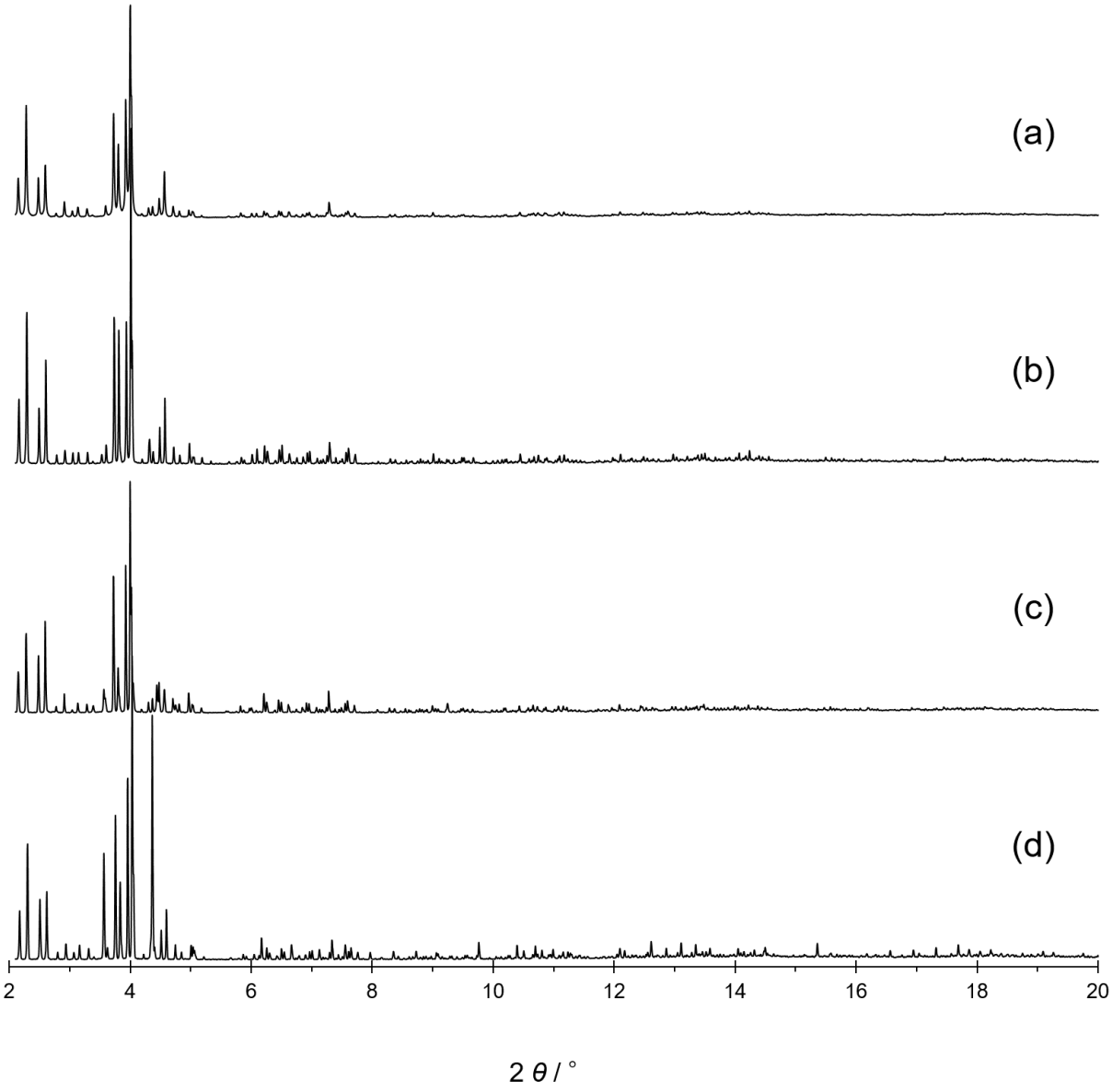

Fig. S10 Powder X-ray diffraction patterns. The observed patterns measured at room temperature (λ = 1.000 Å) for **I** (a), $\mathbf{I_{PF6}}$ (b), $\mathbf{I_{BF4}}$ (c) and $\mathbf{I_{OTf}}$ (d).

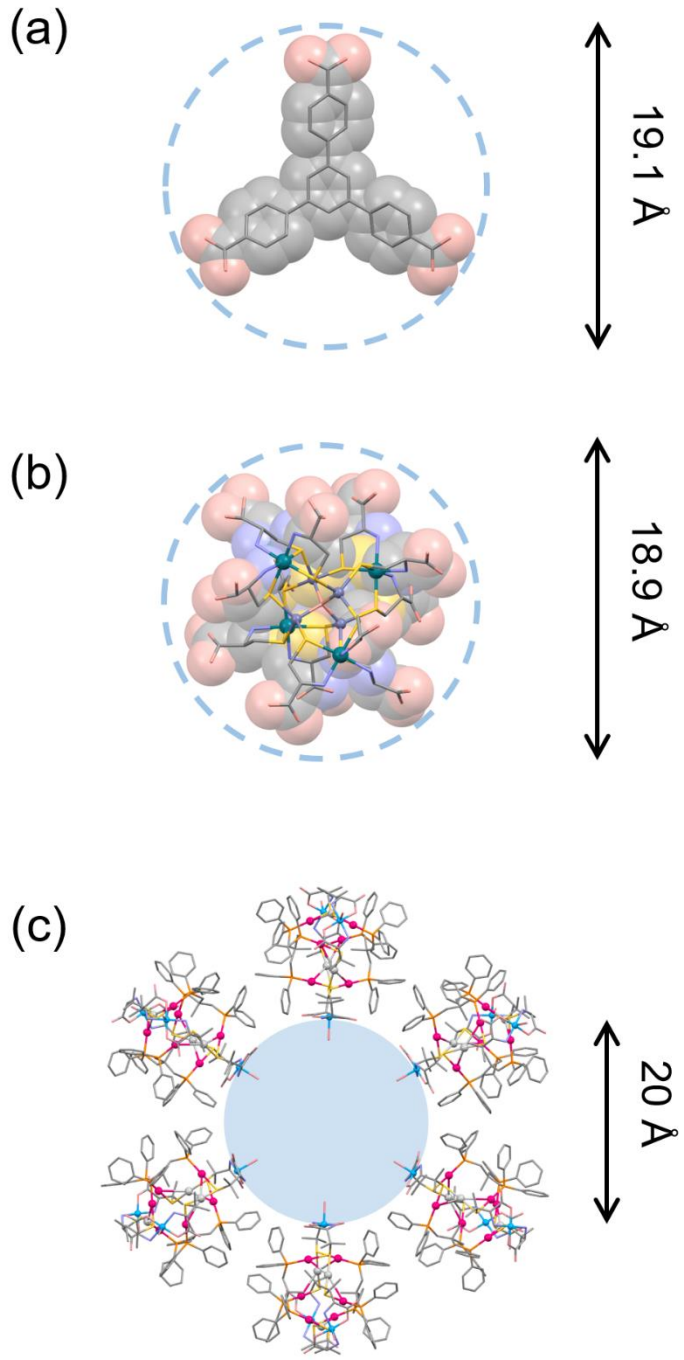

Fig. S11 Molecular structures of BTB^{3-} (a) and $[Rh_4Zn_4O(L\text{-cys})_{12}]^{6-}$ (b), together with the hexagonal window of cage A in **I** (c). [Colour codes: red, Au; silver, Ag; blue, Cu; orange, P; yellow, S; pink, O; pale blue, N; grey, C.] Single-crystal X-ray crystallography of $\mathbf{I_{BTB}}$ and $\mathbf{I_{RhZn}}$ revealed the retention of the single crystallinity and framework structure in **I**.

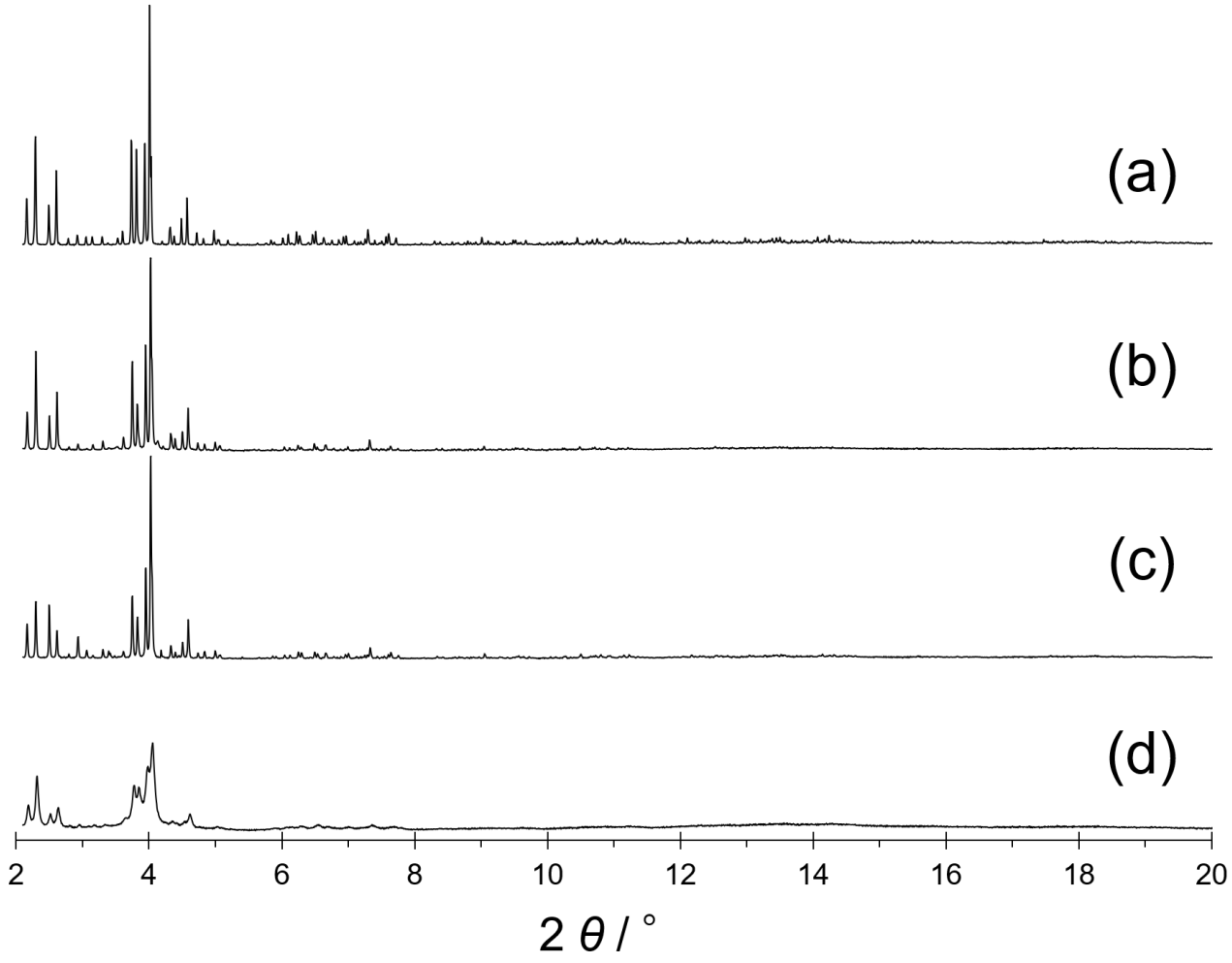

Fig. S12 Powder X-ray diffraction patterns. The observed patterns measured at room temperature (λ = 1.000 Å) for $\mathbf{I_{PF6}}$ (a), $\mathbf{I_{BTB}}$ (b), $\mathbf{I_{RhZn}}$ (c) and $\mathbf{I_{PF6}}$ with Methyl Orange (d).

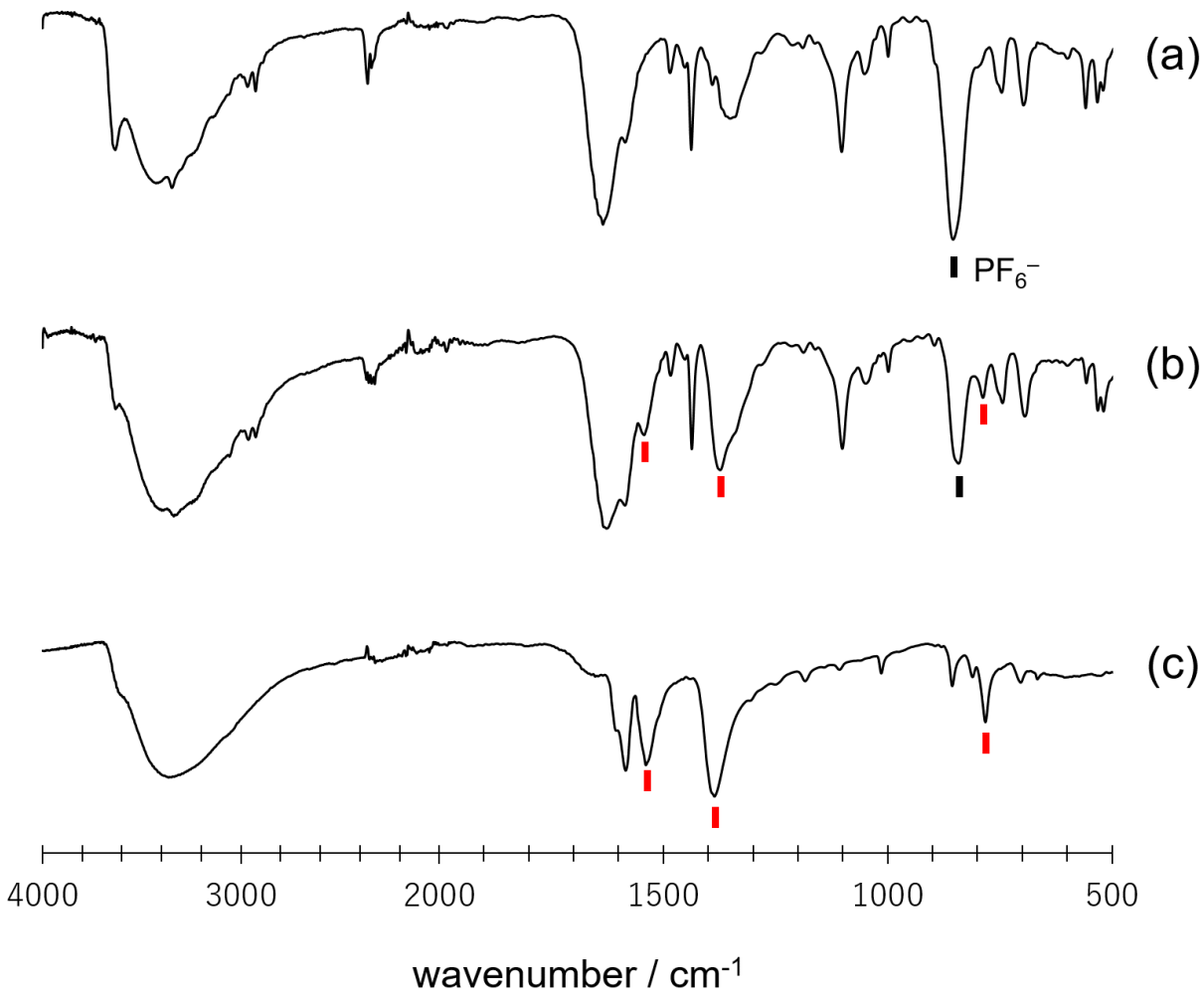

Fig. S13 IR spectra (ATR). $\mathbf{I_{PF6}}$ (a), $\mathbf{I_{BTB}}$ (b), and Na_3BTB (c).

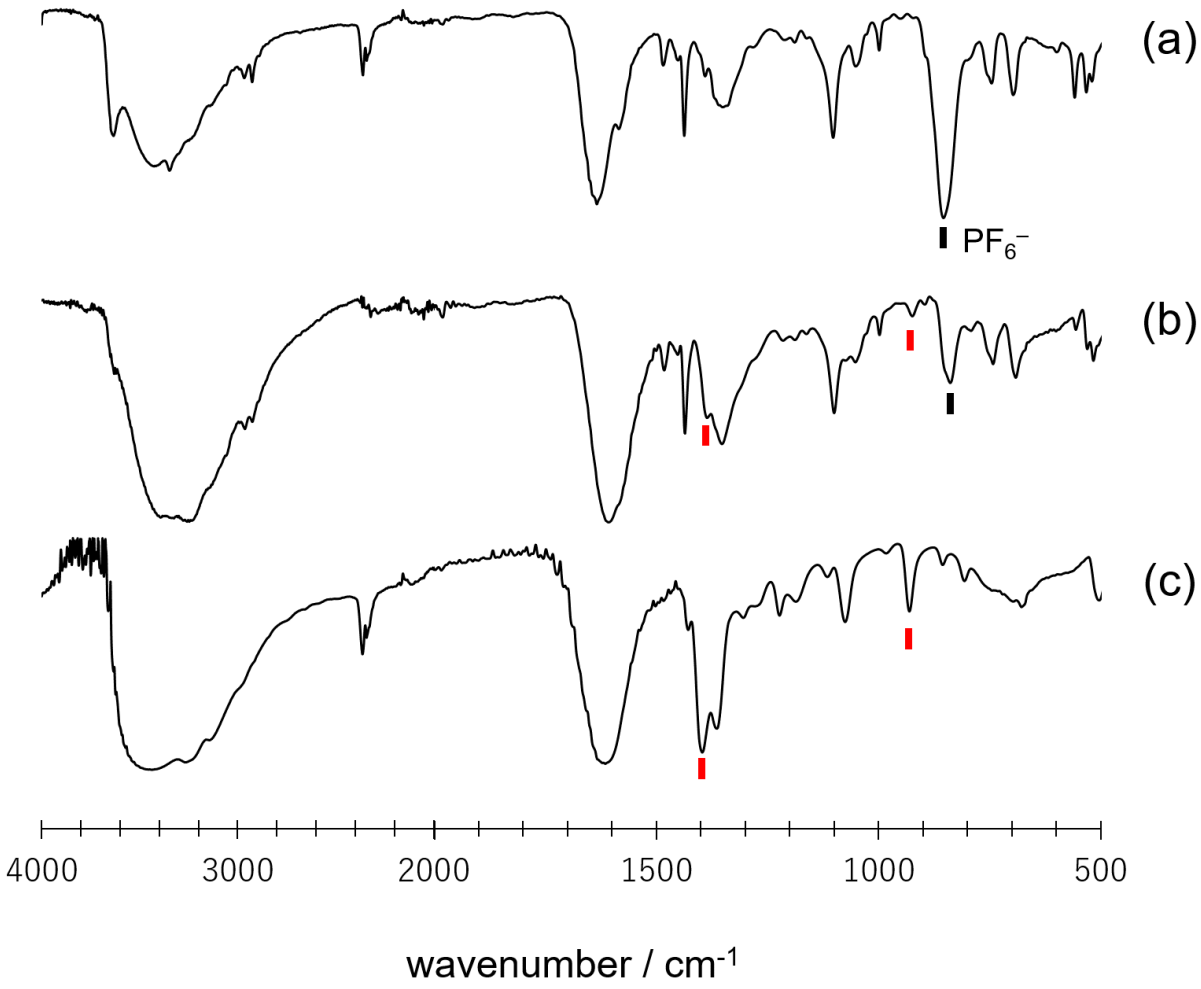

Fig. S14 IR spectra (ATR). $\mathbf{I_{PF6}}$ (a), $\mathbf{I_{RhZn}}$ (b), and $K_6[Rh_4Zn_4O(L\text{-}cys)_{12}]$ (c).

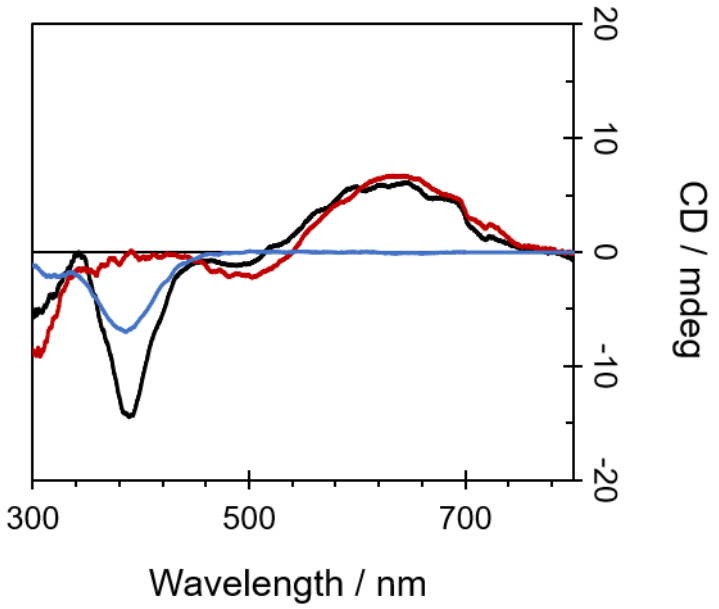

Fig. S15 Solid-state CD spectra. $\mathbf{I_{RhZn}}$ (black), **I** (red) and $K_6[Rh_4Zn_4O(L\text{-}cys)_{12}]$ (blue).

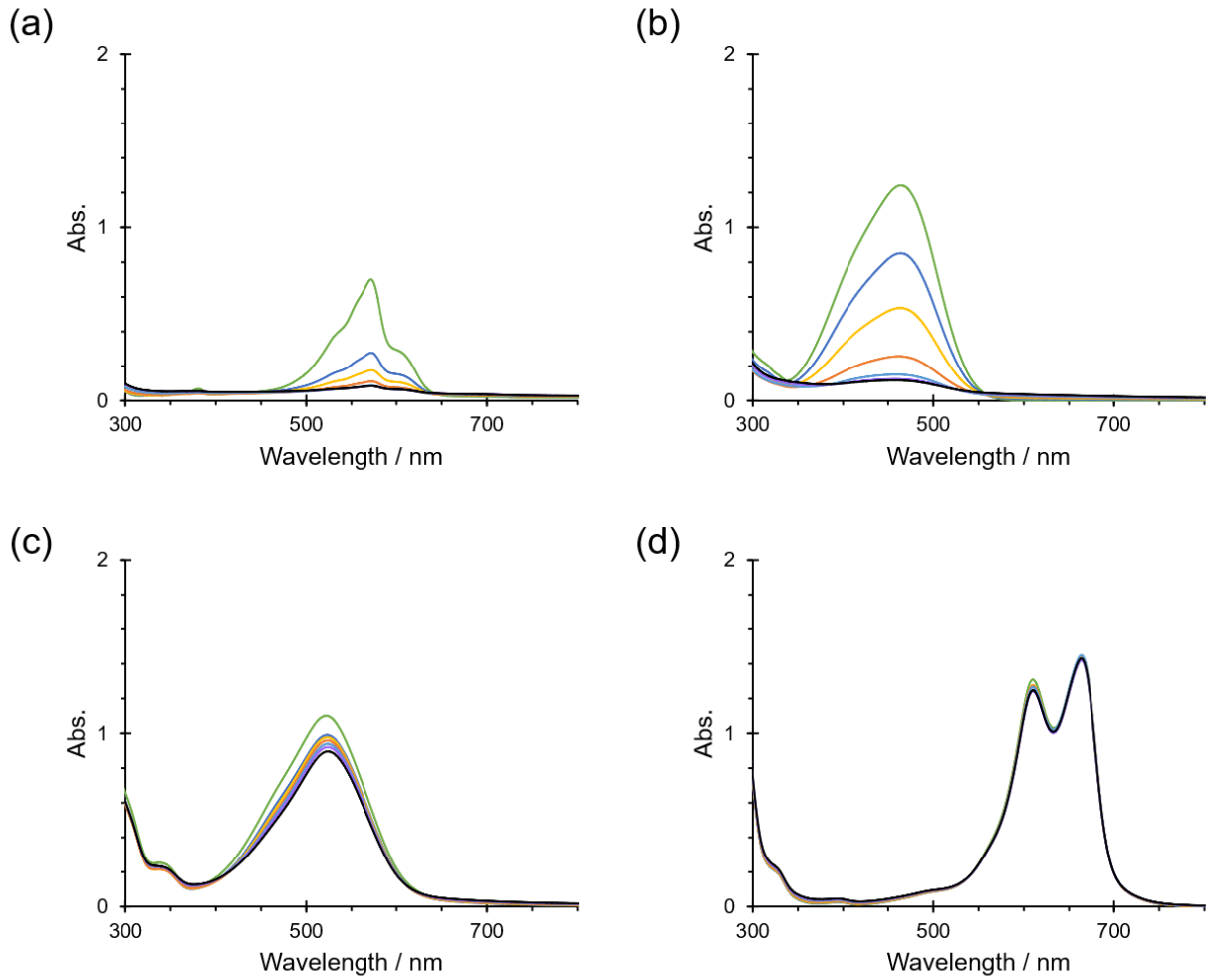

Fig. S16 Time-dependent absorption spectral changes of 1.0 x 10^{-4} M aqueous solutions (3 mL) of Resorufin Sodium (a), Methyl Orange (b), Basic Red 5 (c) and Methylene Blue (d) after soaking crystals of I_{PF6} (~ 5.0 mg) for 0 h (green), 1 h (blue), 2 h (yellow), 4 h (orange), 6 h (light blue), 8 h (purple) and 10 h (black).

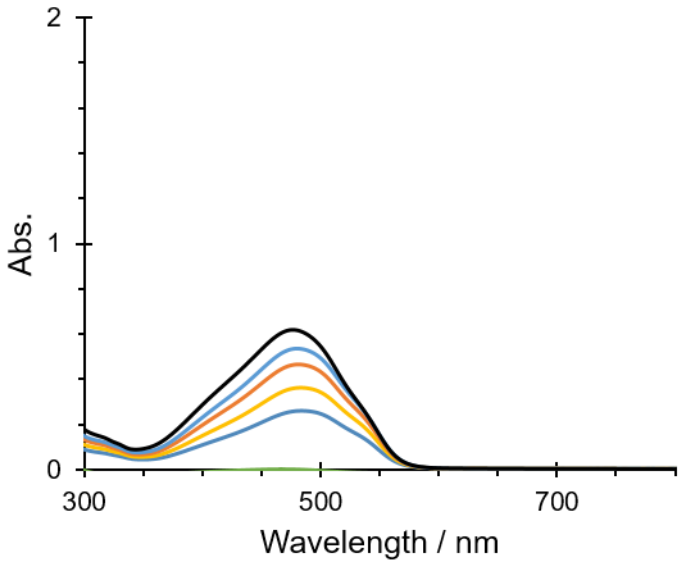

Fig. S17 Time-dependent absorption spectral changes of a 0.2 M aqueous solution of PF_6 after soaking crystals of **I$_{PF6}$** with Methyl Orange (ca. 10.0 mg): 0 h (green), 1 h (blue), 2 h (yellow), 4 h (orange), 6 h (light blue), and 24 h (black).

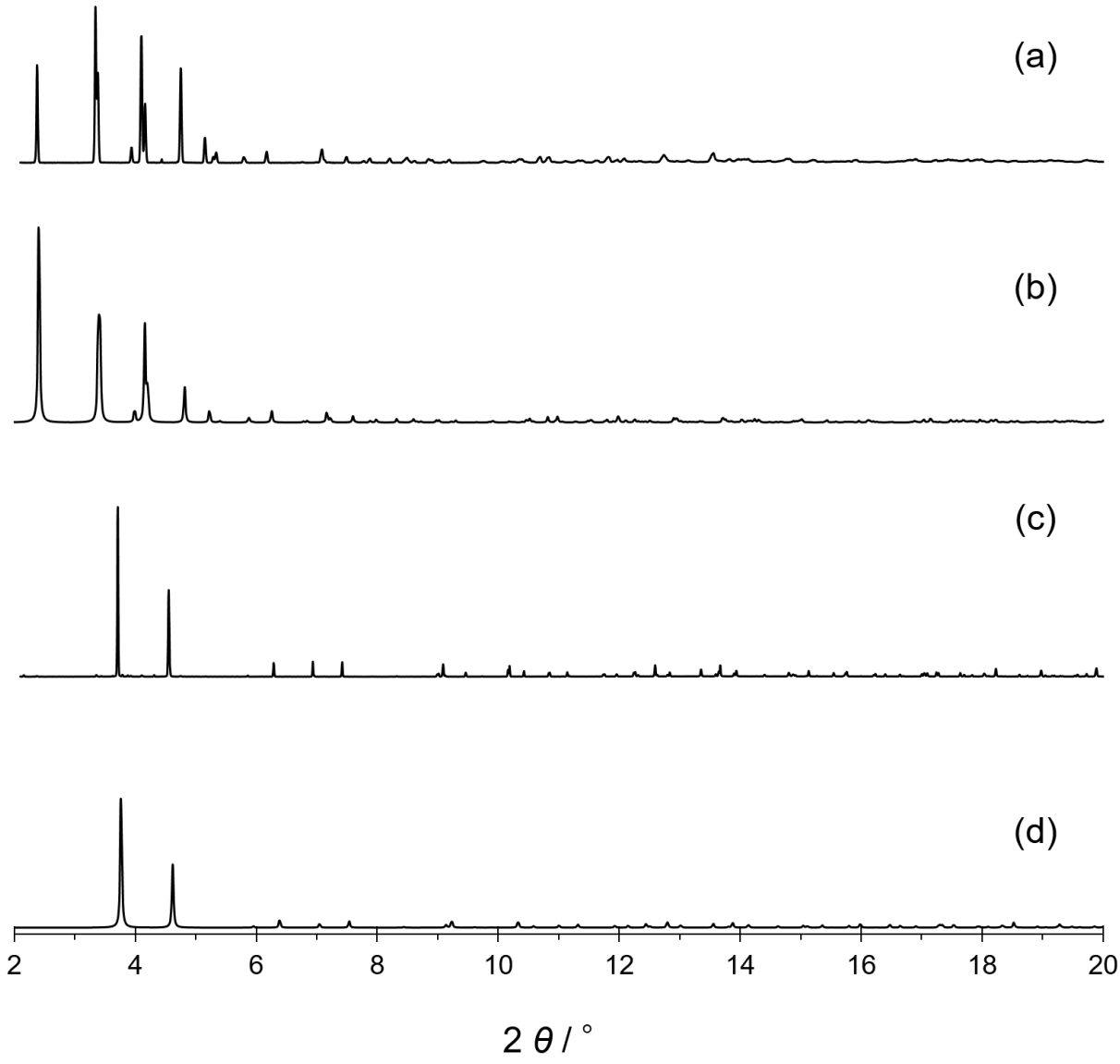

Fig. S18 Powder X-ray diffraction patterns. The observed patterns measured at room temperature (λ = 1.000 Å) for **II** (a) and **II'** contaminated with **II** (c). The simulated patterns for **II** (b) and **II'** (d).

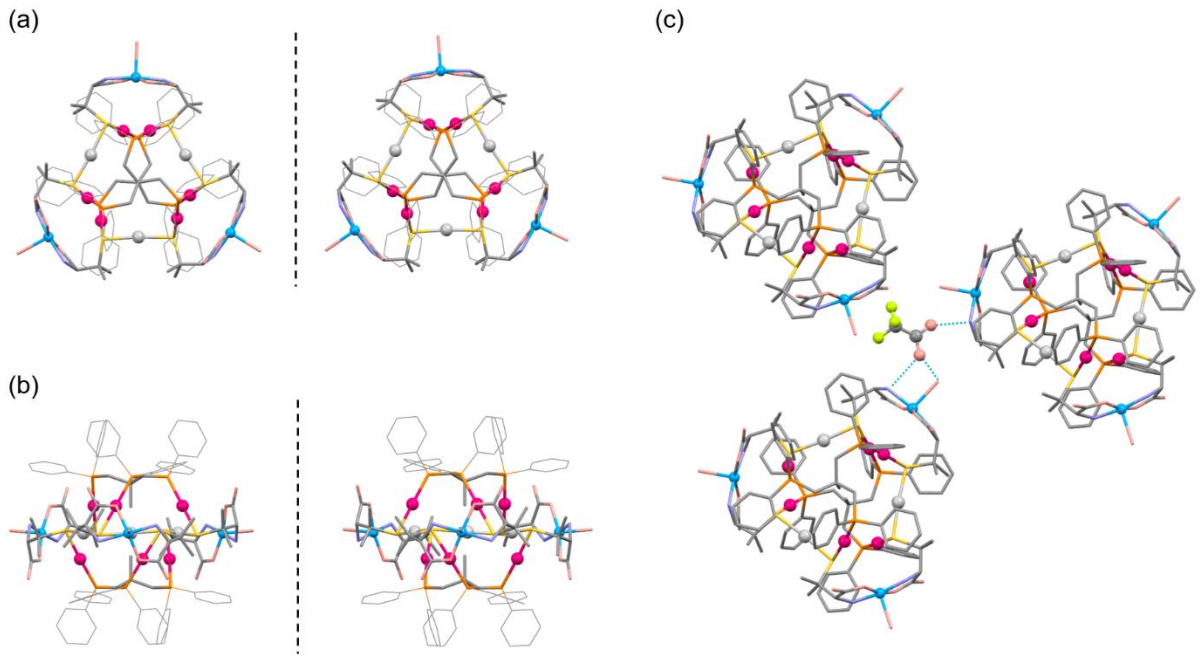

Fig. S19 Crystal structures of **II'**. Top (a) and side (b) views of an enantiomeric pair of $[\mathbf{1^D}]^{3+}$ (left) and $[\mathbf{1^L}]^{3+}$ (right) complex cations. Perspective view of hydrogen-bonding interactions of a TFA^- anion with $[\mathbf{1^D}]^{3+}$ complexes (c). [Colour codes: red, Au; silver, Ag; blue, Cu; orange, P; yellow, S; pink, O; pale blue, N; grey, C. light yellow; F.]

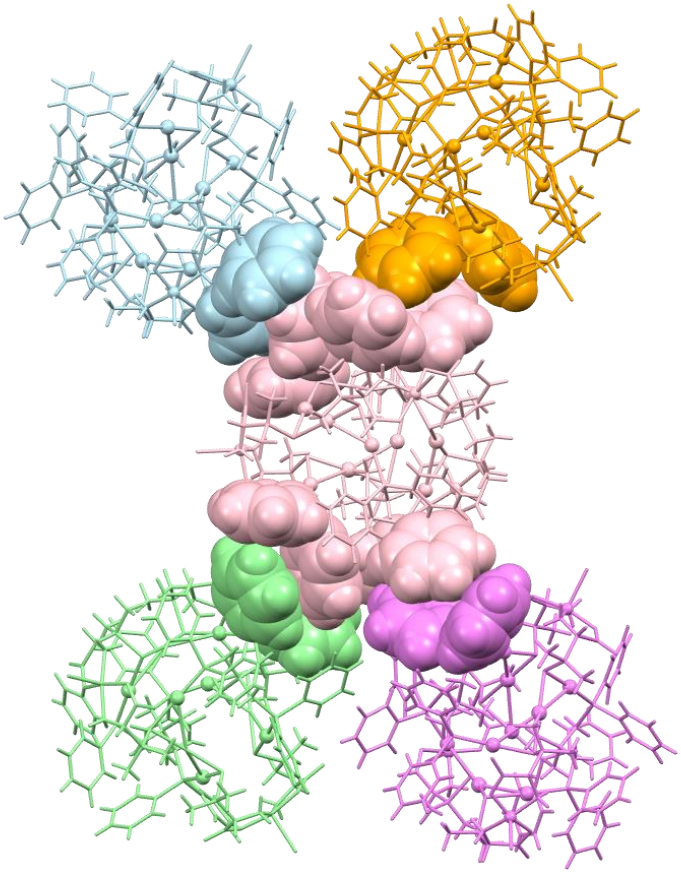

Fig. S20 Perspective view of CH···π interactions through the tdme phenyl groups in **II**.

Table S1. Crystallographic data for $[Ag_3(D\text{-}H_3L^{Au3})_2](NO_3)_3$, **I**, **I'**, **II** and **II'**.

	$[Ag_3(D\text{-}H_3L^{Au3})_2](NO_3)_3$	**I**	**I'**	**II**	**II'**
CCDC No.	2024986	2024987	2024988	2024989	2024990
Formula	$C_{112}H_{172}Ag_3Au_6N_9O_{38}P_6S_6$	$C_{118}H_{172}Ag_3Au_6$ $Cu_3F_9N_6O_{38}P_6S_6$	$C_{118}H_{154}Ag_3Au_6$ $Cu_3F_9N_6O_{29}P_6S_6$	$C_{112}H_{138}Ag_3Au_6$ $Cu_3F_9N_6O_{33.5}P_6S_6$	$C_{118}H_{168}Ag_3Au_6$ $Cu_3F_9N_6O_{36}P_6S_6$
Colour, form	Colourless, Stick	Blue, octahedral	Blue, hexagonal plate	Blue, truncated octahedron	Blue, hexagonal plate
Wavelength/ Å	0.600	0.4281	0.71073	0.62997	0.4281
Crystal system	Orthorhombic	Cubic	Trigonal	Trigonal	Trigonal
Space group	$P2_12_12_1$	$F4_132$	$P321$	$R3$-c	$R3$c
a/ Å	30.1406(4)	129.492(4)	19.2375(4)	33.804(5)	19.2549(7)
b/ Å	32.9119(5)	129.492(4)	19.2375(4)	33.804(5)	19.2549(7)
c/ Å	33.4887(7)	129.492(4)	27.0608(6)	81.734(16)	74.3872(14)
α/ °	90	90	90	90	90
β/ °	90	90	90	90	90
γ/ °	90	90	120	120	120
V/ Å^3	33220.3(10)	2171340(181)	8673.0(4)	80885(28)	23884.2(18)
Z	8	272	2	18	6
T/ K	100(2)	100(2)	100(2)	103(2)	100(2)
F(000)	16096	597040	4210	38700	13050
ρ calcd/ g· cm^{-3}	1.654	0.942	1.672	1.643	1.874
$\mu(\lambda)$/ mm^{-1}	3.585	1.037	5.937	4.016	2.126
Flack parameter	0.012(3)	0.101(7)	0.007(2)	-	0.001(5)
Crystal size/ mm^3	0.07×0.02×0.01	0.23×0.23×0.23	0.20×0.20×0.03	0.05×0.05×0.05	0.12×0.10×0.08
Limiting indices	$-33 \le h \le 33$	$-89 \le h \le 92$	$-23 \le h \le 24$	$-45 \le h \le 49$	$-24 \le h \le 24$
	$-36 \le k \le 36$	$-92\ k \le 92$	$-24 \le k \le 24$	$-51 \le k \le 45$	$-24 \le k \le 24$
	$-37 \le l \le 37$	$-92 \le l \le 92$	$-36 \le l \le 36$	$-123 \le l \le 110$	$-85 \le l \le 96$
R_1 ($I>2\sigma(I)$)[a)]	0.0421	0.1383	0.0240	0.0566	0.0267
Rw_2 (all data)[b)]	0.0977	0.4196	0.0644	0.1950	0.0695
GOF	0.929	1.518	1.048	1.036	1.032